J Mater Sci (2010) 45:6599–6603
DOI 10.1007/s10853-010-4749-0

Oriented growth of piezoelectric crystallites at the normal direction of glass cylinders

Fei Duan · Bin He

Received: 14 April 2010 / Accepted: 1 July 2010 / Published online: 14 July 2010
© Springer Science+Business Media, LLC 2010

Abstract The oriented crystallites were found to grow from the cylindrical surface toward inside at the normal direction during the crystallization in the BaO–SrO–TiO_2–SiO_2 glass. The oriented growth in the cylinders was consistent with the heat transfer direction in the post-thermal treatment, in which the temperature was rapidly increased from the transition point of the glass to the point for the bulk crystallization in a precisely temperature-controlled furnace. The crystalline phase, $(Ba_{0.2}Sr_{1.8})TiSi_2O_8$, was evenly embedded in the glass phase in the non-ferroelectric piezoelectric glass ceramics. The cylinders with oriented crystallization can be machined into the piezoelectric tubes with radial polarization.

Introduction

The growth of non-ferroelectric piezoelectric crystallites in the glass can resulted in the oriented functional glass ceramics, which have demonstrated piezoelectric, electro-optical, and pyroelectric properties in the systems of $Li_2Si_2O_5$, $Li_2B_2O_7$, $Ba_2TiGe_2O_8$, $Ba_2TiSi_2O_8$, and $Sr_2TiSi_2O_8$ [1−6]. The glass ceramics, having no aging and depolarization problems, own a high hydrostatic piezoelectric coefficient, proper density, mechanical flexibility, and a low-dielectric coefficient. The disk-shaped elements were tested and found to be applicable for such electromechanical devices as hydrophone [5, 6]. Different from the disk-shaped elements, the tube-shaped elements with radial polarization, nearly omnidirectional in constructing a sensor or actuator, can provide highly efficient electromechanical energy conversion and produce little distortion in the acoustic field [7−13]. However, most tube-shaped elements are ferroelectric at present and not active before they are polarized. Therefore, the reliability is affected by depolarizing, and the re-polarization process increases the complexity and cost. The oriented growth of $Ba_2TiSi_2O_8$ crystallites in the glass can form a functional composite with the acicular aligned piezoelectric crystallites distributing in the residual glass matrix phase. A driven force was believed as the maintained large temperature gradient created on a hot stage [14], on which the temperature field was not easy to control. Wisniewski et al. studied the crystallization of the $2BaO–3TiO_2–2.75SiO_2$ glass at 810 °C [15]. Only about 60 μm orientated layer of the fresnoite crystallites was formed due to surface nucleation. The fresnoite crystallites were randomly oriented at a depth greater than 60 μm due to volume nucleation. They also investigated the electrochemically induced nucleation, which led to the rectangular shaped dendritic growth [16]. The surface nucleation is shown to be important to obtain an oriented growth of the crystallites. In addition, as indicated in Fig. 1a, the glass in the BaO–SrO–TiO_2–SiO_2 system can crystallize from the periphery of cubic glass to inside in an electric furnace under a predetermined post-thermal treatment introduced in "Experimental procedure" section. Therefore, it provides us a way to produce the oriented crystallization with the surface nucleation in the glass with particular configurations, such as cylinder, sphere, etc. Addressed in the paper, the oriented crystallization in the cylindrical rods from the BaO–SrO–TiO_2–SiO_2 glass was investigated by controlling the glass formation, determining the crystalline phase, measuring the microstructure, and fabricating the piezoelectric tubes.

F. Duan (✉) · B. He
School of Mechanical and Aerospace Engineering, Nanyang Technological University, Singapore 639798, Singapore
e-mail: feiduan@ntu.edu.sg

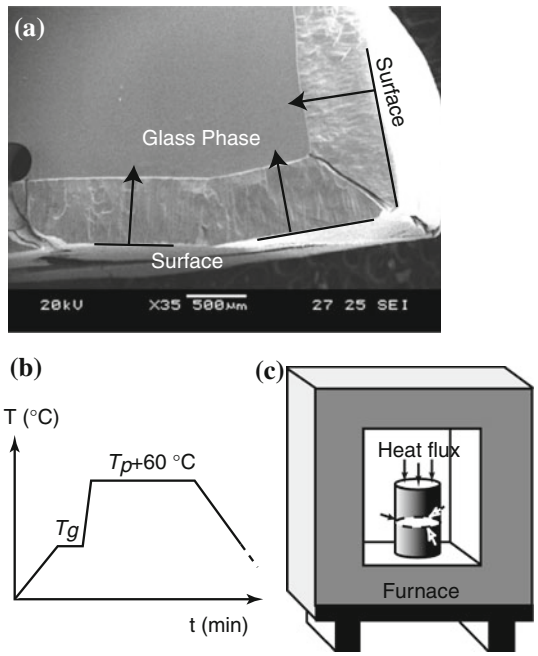

Fig. 1 The microstructure in the cross section of the half crystallized glass cube in the $(SrO)_{1.8}(BaO)_{0.2}(TiO_2)_{1.0}(SiO_2)_{2.9}$ glass is illustrated in (**a**) under the scanning electron microscope (SEM). The post-thermal treatment schematic for crystallization is shown in (**b**). A cylindrical glass rod is in the post-thermal treatment in a furnace displayed in (**c**)

Experimental procedure

The oriented crystallization in the piezoelectric glass ceramics required a heterogenous nucleation at the surface and rapid growth in the glass system [17]. Recent development on the crystallization techniques in the BaO–SrO–TiO_2–SiO_2 glass cube can help us to have the oriented crystallization in a glass bulk with a curved surface. The glass in the system of 0.2BaO–1.8SrO–TiO_2–2.9SiO_2 was selected to keep the solid solution crystalline phase of $Ba_{0.2}Sr_{1.8}TiSi_2O_8$ in the glass ceramics, because the glass ceramics have a higher piezoelectric coefficient, d_{33} [3, 5]. The reagent grade chemicals of 1.8$SrCO_3$, 0.2$BaCO_3$, 1.0TiO_2, and 2.9SiO_2 (in molar ratio) were mixed with a small amount of $CaCO_3$ to enhance the glass forming by reducing the melting viscosity [18]. The well-mixed chemicals were melted at 1520 °C and quenched to form fully transparent glass cylindrical rods with a light brown color. The glass rods were then annealed at 600 °C. In order to determine the glass transition temperature (T_g) and crystallization temperature (T_p), the glass was ground into fine powder for the differential thermal analysis (DTA, Parkin Elmer DTA7) at a scanning rate of 20 °C/min from the room temperature to 1000 °C. The post-thermal treatment route could be determined as a result, as shown in Fig. 1b. The glass cylinders with the different diameters were treated for the crystallization in a precisely temperature-controlled furnace, shown in Fig. 1c. Following the post-thermal treatment route, the glass cylinders were preheated to T_g from room temperature at 5 °C/min at first and maintained there for about 10 min for surface nucleation. Afterward, the furnace temperature was increased at a rate of 20 °C/min to the temperature for crystallization, 60 °C above the crystallization temperature (T_p) from the DTA curve, and kept for 3 h. The bulk crystallization temperature with 60 °C higher in the glass would result in a fast crystallization from the surface of the glass cylinders to inside, but would not deform the surface of the glass cylinder. The crystalline phase in the studied materials was determined in the ground powder by using the X-ray diffraction method in the scanning angle of 10°–70° (XRD, Philips PW1820). In order to observe the microstructure under a scanning electron microscopy (SEM, Jeol JSM - 5600LV), the glass-ceramic cylinders were broken in the radial direction, then the broken surface was etched in 1% hydrofluoric acid for 2 min, and coated with Au. Although the glass ceramics are a kind of brittle materials, they exhibit good thermal shock resistance and mechanical toughness when compared to their base glass since the glass ceramics are a composite of the crystallites and the residual glass phase. Thus, the piezoelectric tube can be machined by the diamond tools from the glass-ceramic cylindrical rods. The cylinders were cut into a predetermined length, drilled at the centerline, ground into tubes with a certain wall thickness. Then silver electrodes were coated at both the inside and outside of the tubes. An HP4192 impedance analyzer was applied to measure the dielectric and piezoelectric properties.

Results and discussion

The inset in Fig. 2 is the DTA spectrum of the glass powder shown from 600 to 1000 °C at an increasing temperature rate at 20 °C/min. It is indicated that the glass transition temperature, T_g is at 760 °C, and the crystallization temperature, T_p is at 900 °C. Thus, the post-thermal treatment temperature for the bulk crystallization in the glass was set at 960 °C consequentially as illustrated in Fig. 1b. That only one exothermic peak is found up to 1000 °C suggests that only a single phase was crystallized from the glass if no exothermic peaks overlaps. Heating the glass cylindrical rods with the different diameters at 760 °C for 10 min was for the surface nucleation, then the furnace temperature was increased to 960 °C at 20 °C/min for the oriented crystallization. The materials then became opalescent in color and was not transparent any more. The XRD spectrum of the glass ceramics is compared with those of the glass and the JCPDS card (No. 022-0513), as illustrated in Fig. 2. Note that no characteristic peaks of

crystalline phases are found in the glass sample, but the peaks in the glass ceramics demonstrate that there is a crystalline phase, which is similar to the fresnoite single crystal identified in the JCPDS card and the other researches [3, 19]. A little angle migration of the characteristic peaks suggests that a solid solution was formed in the glass ceramics. If combining the XRD spectra with the DTA result, it is concluded that the crystalline phase was a single phase $Ba_{0.2}Sr_{1.8}TiSi_2O_8$ in the glass ceramics. Although the molar ratio of Ba:Sr:Ti:Si in the glass was purposely set to 2:18:10:29 to improve the glass forming, the molar ratio of the piezoelectric crystalline phase is 2:18:10:20. The superfluous SiO_2 should be in the residual glass phase. The base glass is a non-stoichiometric fresnoite-like system, similar to the system introduced by Wisniewski et al. [15]. Cabral et al. measured the internal homogeneous nucleation rates and crystallite growth in the stoichiometric fresnoite glass [20, 21]. The temperature in the post-thermal treatment was below 750 °C, much lower than the bulk crystallization temperature in this study. Their crystallization rates were relatively slow, as observed in the radial direction of the crystallites. The oriented growth has not been reported.

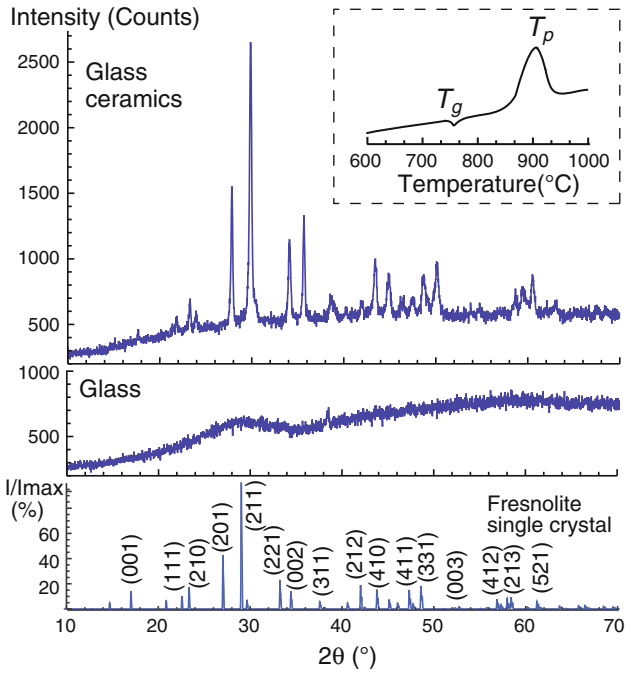

Fig. 2 The powder XRD spectra of the glass and the glass ceramics. The DTA curve of the glass in the inset

Figure 3 demonstrates the glass-ceramic micrographs, the oriented acicular crystallites grew toward the center of the cylinders perpendicularly to the tangential direction of the curved surface. The oriented depth is greater than 0.7 mm from the circular surface in the 7.6-mm diameter cylinder in Fig. 3a. The oriented distance could reach about 1.0 mm, but it cannot be shown in the single image. As seen there, the oriented degree of the crystallites becomes worse with an increase of the depth from the cylindrical surface to inside. The trend is more distinct in the glass-ceramic cylinder with a diameter of 1.2 mm in Fig. 3b. In the small cylinder, the oriented degree is good as the depth is less than 0.3 mm, while the oriented degree becomes worse as the depth is larger than 0.3 mm. One of possible reasons is the curvature effects, denoted by $1/R$ (R is the radius of the cylinders). The curvature of the 1.2-mm diameter cylinder is 6.3 times as large as that in the 7.6-mm diameter cylinder. A larger curvature would induce a disturbance between two neighboring long acicular crystallites during growing. Another reason might be from heat transfer in the cylinders. In the furnace, the rapid temperature increase from 760 to 960 °C would generate a large temperature gradient toward the centerline of the glass cylinders from the surface initially. The centerline temperature would approach the temperature at 960 °C with time during the experiment. Thus, the temperature gradient would became smaller in the process. However, the time periods to reach the uniform temperature would be different in the cylinders with the different diameters. Note that the oriented growth is the same direction as the temperature gradient in the glass rods during the post-thermal treatment as same as that on the hot stage indicated by Halliyal et al. [14]. We can estimate heat transfer in the glass cylinders if account of the heat release during the crystallization is not taken into. Simply analyzing, we can simulate that a glass

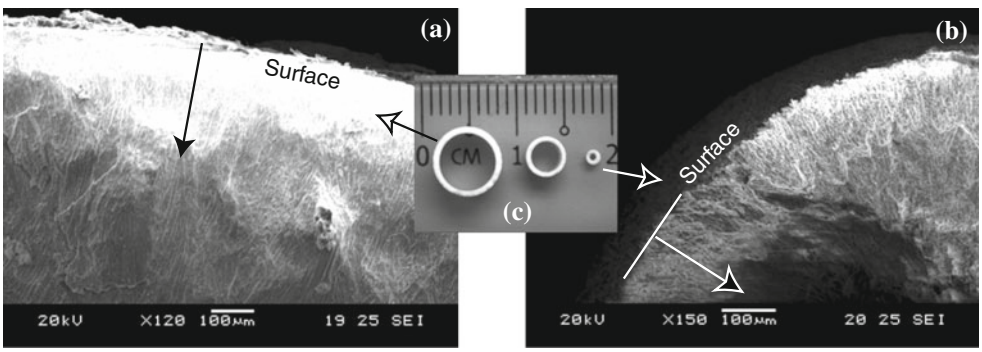

Fig. 3 SEM micrographs of cylindrical glass ceramics in the cross section, 7.6 mm in diameter (**a**), 1.2 mm in diameter (**b**). The composites were fabricated into the hollow tubes as shown in (**c**)

cylinder at T_1 (760 °C) is suddenly put in a furnace which is maintained at a high temperature of T_2 (960 °C), heat transfer in the cylinder could be explained by the constant convective boundary conditions.

The transient heat transfer in a solid glass cylinder with a radius of R is expressed as,

$$\frac{\partial^2 T}{\partial r^2} + \frac{1}{r}\frac{\partial T}{\partial r} = \frac{1}{\alpha}\frac{\partial T}{\partial t}, \tag{1}$$

with the boundary and initial conditions,

$$T(r,0) = T_1, \tag{2}$$

$$\left.\frac{\partial T(r,t)}{\partial r}\right|_{r=0} = 0, \tag{3}$$

$$h[T(R,t) - T_2] = \kappa \left.\frac{\partial T(r,t)}{\partial r}\right|_{r=R}, \tag{4}$$

where r is the radial distance from the centerline of cylinder ($0 \le r \le R$), α is the thermal diffusivity, κ is the thermal conductivity, and h is the heat convection coefficient in the furnace. The solution solved with separation of variables can be written as,

$$T(\eta,t) = T_2 + (T_1 - T_2) \times \sum_{m=1}^{\infty} \frac{2}{\mu_m} \frac{J_1(\mu_m) J_0(\eta\mu_m)}{J_0^2(\mu_m) + J_1^2(\mu_m)} e^{-\mu_m^2 F_0}, \tag{5}$$

where the term $\mu_m J_1(\mu_m) = \frac{hR}{\kappa}$ can be solved mathematically, $F_0 = \frac{\alpha t}{R^2}, \eta = \frac{r}{R}$. As $F_0 > 0.2$, neglecting the terms except the first term as $m = 1$ only results in less than 2% error [22]. Therefore, the temperatures at the centerline can be simplified as,

$$T(0,t) = T_2 + (T_1 - T_2)\left(\frac{2}{\mu_1} \frac{J_1(\mu_1)}{J_0^2(\mu_1) + J_1^2(\mu_1)}\right) e^{-\mu_1^2 F_0}. \tag{6}$$

If the physical and thermal properties (thermal diffusivity, thermal conductivity, and convective heat transfer coefficient) in the calculation were selected at (860 °C) [23, 24], the temperature at the centerline of cylinders could be calculated and illustrated in Fig. 4. As shown there, to reach 960 °C from 760 °C at the centerline, the time required in the 10.0-mm diameter glass cylinder is above 20,000 s. The time period decreases with a decrease of the cylinder diameter, about 5,600 s within the 1.2 mm-diameter glass cylinder. Since the furnace temperature field would not observably be disturbed if the cylinders (in millimeter scale) are put into the furnace chamber (in a decimeter scale), we can assume the air temperature around the cylinders, T_{air}, is kept at 960 °C all the time. Therefore, the average temperature gradient, $\overline{q}$, expressed in Eq. 7, can qualitatively be applied to explain the oriented crystallization.

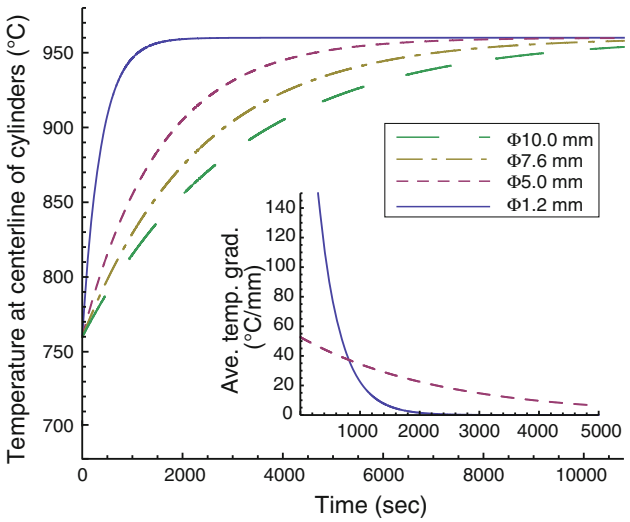

Fig. 4 The centerline temperature in the cylinders with the diameter at 1.2, 5.0, 7.6, and 10.0 mm as a function of time. The average temperature gradient from the centerline of the cylinder to the position of T_{air} is shown in the inset for the cylinder of 1.2 and 7.6 mm

$$\overline{q} = \frac{T_{air} - T(0,t)}{R^+}, \tag{7}$$

where R^+ is the distance from the centerline of a glass cylinder to the position of T_{air} at 960 °C.

The initial average temperature gradient in the 7.6-mm cylinder is 52.7 °C/mm, less than one sixth of that in the 1.2-mm cylinder. A quick loss is found in the average temperature gradient at the 1.2-mm cylinder, however, the decreasing temperature gradient at the 7.6-mm cylinder is relative slow as illustrated in the inset of Fig. 4. After a certain time at around 800 s, the average temperature gradient in the 7.6-mm cylinder becomes larger than that in the 1.2-mm cylinder. It might be another reason to explain that a better oriented growth degree is observed at the outer region of the glass cylinder with a 1.2-mm diameter but not at the inside.

Besides the effects of the temperature gradient on the oriented crystallization, the mechanical constrain can be explained for the oriented crystallization. Although the mechanical constrain was to release at T_g by keeping 10 min in this study, the mechanical strain can be produced in the quick temperature increase at 20 °C/min, especially when the glass was crystallized from the surface to the inside of the glass cylinders. The induced stains in the normal direction of the cylinder, imposed by the mechanical constraints during the crystallite growth [25], can enhance the orientation of crystallites. In addition, if the thermal expansion of the crystallites and the glass phase is different, the stains can act on the piezoelectric crystallites to generate an electric field during the crystallization. The

electric field might also reinforce the oriented crystallite growth, as reported by Wisniewski et al. [16].

Shortly, the oriented crystallization in the glass system could be resulted from the temperature gradients from heat transfer in the cylinders, mechanical constrain, electric field, etc. The cylindrical piezoelectric composite can be machined into tubes as shown in Fig. 3c. The preliminary measurement of a tube with radial polarization (7.6 mm in outer diameter, 6.0 mm in inner diameter, 7.0 mm in height) shows that the relative dielectric constant is 17.0 and piezoelectric coefficient of d_{31} is 1.4×10^{-12} C/N.

Conclusions

The oriented $Ba_{0.2}Sr_{1.8}TiSi_2O_8$ crystallites are observed to grow from the surface to inside at the normal direction of the glass cylinders (Figs. 2, 3) under a designed post-thermal treatment in Fig. 1b. The crystallite growth direction in the cylinders is found to be in consistence with the direction of heat transfer. The cylinders can then be machined into thin wall tubes with radial polarization. By applying the oriented crystallization techniques from the curved surface reported in the paper, the non-ferroelectric oriented glass ceramics can be made into such particular configurations as hollow spherical shells, conical and cylindrical tubes, etc. with positive or negative polarization at the normal direction of the curved surface.

Acknowledgement The authors would like to acknowledge the support of the staff in Materials Lab at School of Mechanical and Aerospace Engineering, Nanyang Technological University.

References

1. Gardopee GJ, Newnham RE, Halliyal A, Bhalla AS (1980) Appl Phys Lett 36:817
2. Davis MJ, Vullo P, Mitra I, Blaum P, Gudgel KA, Donnelly NJ, Randall CA (2008) J Am Ceram Soc 91:2878
3. Halliyal A, Safari A, Bhalla AS, Newnham RE, Cross LE (1984) J Am Ceram Soc 67:331
4. Halliyal A, Bhalla AS, Cross LE, Newnham RE (1985) J Mater Sci 20:3745. doi:10.1007/BF01113783
5. Duan F, Fang C, Ding Z (1998) Mater Lett 34:184
6. Ting RY, Halliyal A, Bhalla AS (1984) Appl Phys Lett 44:852
7. Lewis RWC, Bowen CR, Dent ACE, Jonas K (2009) Ferroelectrics 389:95
8. Huang CH, Lin YC, Ma CC (2004) IEEE Trans Ultrason Ferroelectr Freq Control 51:12
9. Drumheleer DS, Kalnins A (1970) J Acoust Soc Am 47:1343
10. Adelman NT, Stavsky Y, Segal E (1975) J Sound Vib 38:245
11. Alkoy S (2007) J Mater Sci 42:6742. doi:10.1007/s10853-006-1477-6
12. Kiekczyński P, Pajewski W, Szalewski M (2002) J Appl Phys 91:10181
13. Zhang QM, Wang H, Cross LE (1993) J Mater Sci 28:3962. doi:10.1007/BF00353206
14. Halliyal A, Bhalla AS, Newnham RE, Cross LE (1981) J Mater Sci 16:1023. doi:10.1007/BF00542748
15. Wisniewski W, Nagel M, Volksch G, Russel C (2010) Cryst Growth Des 10:1414
16. Wisniewski W, Nagel M, Volksch G, Russel C (2010) Cryst Growth Des 10:1939
17. Uhlmann DR (1985) J Non-Cryst Solids 73:585
18. Angeli F, Gaillard M, Jollivet P, Charpentier T (2007) Chem Phys Lett 440:324
19. Lee HK, Lee YS, Bhalla AS, Kang WH (2006) Mater Lett 60:2457
20. Cabral AA, Fokin VM, Zanotto ED, Chinaglia CR (2003) J Non-Cryst Solids 330:174
21. Cabral AA, Fokin VM, Zanotto ED (2004) J Non-Cryst Solids 343:85
22. Çengel YA (2006) Heat and mass transfer: a pratical approach, 3rd edn. McGraw-Hill, New York, p 230
23. Fanderlik I (1991) Silica glass and its application. Elsevier, New York, p 229
24. Martynenko OG, Khramtsov PP (2005) Free-convective heat transfer: with many photographs of flows and heat exchange. Springer, Berlin, p 293
25. Burfoot JC, Taylor GW (1979) Polar dielectrics and their applications. The MacMillan Press LTD, London, p 29